M&C 2017 - International Conference on Mathematics & Computational Methods Applied to Nuclear Science & Engineering, Jeju, Korea, April 16-20, 2017, on USB (2017)

Uncertainty Quantification of the BEAVRS Benchmark Problem at the Steady State

Chenghui Wan, Liangzhi Cao, Hongchun Wu

Xi'an Jiaotong University, No. 28 Xianning West Road, Xi'an, Shaanxi Province, 710049, caolz@mail.xjtu.edu.cn

Abstract – *In this paper, the uncertainty-analysis capability based on the "two-step" scheme for the reactor-physics calculations has been complemented in our home-developed NECP-UNICORN code. The Bamboo code package developed by NECP laboratory of Xi'an Jiaotong University is applied in NECP-UNICORN for the reactor-physics calculations. The Bamboo-Lattice is applied for the lattice calculations and Bamboo-Core for the core simulations. Using NECP-UNICORN, uncertainty analysis based on the statistical sampling method has been applied to the steady-stated BEAVRS benchmark for both the ARI and ARO conditions. For the uncertainty analysis to the lattice calculations, the nuclear-data uncertainties of the main isotopes are propagated to the eigenvalue and few-group constants of different fuel assemblies; for the uncertainty analysis to the core simulations, the uncertainties existed in the few-group constants are propagated to the important responses of the core simulations, including the multiplication factor and power distributions. From the numerical results of uncertainty analysis to the lattice calculations, it can be observed that the relative uncertainties existed in the eigenvalues of different fuel assemblies vary from 5.0‰ to 5.7‰; and the largest relative uncertainties of the two-group constants can up to be 1.70% for D_1(the diffusion cross section of the fast group). From the numerical results of uncertainty analysis to the steady-stated core simulations, it can be observed that the relative uncertainties are about 5.1‰ for the ARO situation and 5.0‰ for the ARI situation, which are the same magnitude of the relative uncertainties of the eigenvalues of the fuel assemblies; for the radial power distributions, the relative uncertainties can up to be 4.27% as the maximum value and 2.08% as the RMS value for the ARO situation, and 6.03% as the maximum value and 2.37% as the RMS value for the ARI situation*.

I. INTRODUCTION

In this paper, the capability of uncertainty analysis has been implemented in our home-developed code NECP-UNICORN based on the statistical sampling method (SSM), propagating the nuclear-data uncertainties to the important responses of the reactor-physics calculations. The "two-step" scheme has been applied in NECP-UNICORN to perform the uncertainty analysis for the reactor-physics calculations. For uncertainty analysis to the lattice calculations, the nuclear-data uncertainties are propagated to the important responses, including the eigenvalue, few-group constants, kinetic parameters and atomic densities; then for uncertainty analysis to the core simulations, the uncertainties of the multiplication factor, power distributions, Boron curve and AO curve introduced by the few-group constants' uncertainties can be quantified. The Bamboo code package developed by Xi'an Jiaotong University has been coupled into NECP-UNICORN to perform the reactor-physics calculations, with Bamboo-Lattice for the lattice calculations and Bamboo-Core for the core simulations. Applying the NECP-UNICORN code, the uncertainty analysis has been performed to the BEAVRS benchmark problem at the Hot Zero Power (HZP) conditions, with situations of All Rod In (ARI) and All Rod Out (ARO). Before the uncertainty analysis to the BEAVRS benchmark, verification of the modeling and simulations based on the Bamboo code package has been performed, using the results obtained by CASMO5 done and published by Idaho National Laboratory (INL). Based on the verification of modeling and simulations of the BEAVRS benchmark using Bamboo, the uncertainty analysis has been performed: for the lattice calculations, the relative uncertainties of the eigenvalues and few-group constants introduced by the nuclear-data uncertainties of the main isotopes are quantified for different the fuel assemblies; for the steady-stated core simulations, the relative uncertainties of the multiplication factor and power distributions has been quantified.

From the numerical results of uncertainty analysis to the lattice calculations, it can be observed that the relative uncertainties existed in the eigenvalues of different fuel assemblies vary from 5.0‰ to 5.7‰; and the largest relative uncertainties of the two-group constants can up to be 1.70% for D_1(the diffusion cross section of the fast group). From the numerical results of uncertainty analysis to the steady-stated core simulations, it can be observed that the relative uncertainties are about 5.1‰ for the ARO situation and 5.0‰ for the ARI situation, which are the same magnitude of the relative uncertainties of the eigenvalues of the fuel assemblies; for the radial power distributions, the relative uncertainties can up to be 4.27% as the maximum value and 2.08% as the RMS value for the ARO situation, and 6.03% as the maximum value and 2.37% as the RMS value for the ARI situation.

This paper is organized as follow. The brief introduction to the theories and methods are presented in section II-1. Section II-2 shows the results and conclusions, including verifications of the modeling and simulations for the BEAVRS benchmark based on Bamboo code package

and the uncertainty results for the lattice calculations and steady-stated core simulations.

II. DESCRIPTION OF THE ACTUAL WORK

With the increasing demand for the best-estimate predications to be provided with their confidence bounds in the nuclear research, industry, safety and regulation, the OECD/NEA has organized the UAM ("Uncertainty Analysis in Modeling") expert group to establish the benchmarks for the uncertainty analysis for the coupled multi-physics and multi-scale LWR system [1]. In the reactor system, the reactor-physics calculation is the prerequisite for the nuclear safety, reactor design and radiation shielding analysis, which requires the nuclear data as the fundamental input parameters. With the increasing development of the advanced methods for the reactor-physics calculations and simulations, the accuracy of the reactor-physics calculation is mainly limited by the precision of the input parameters, especially the nuclear data. Moreover, the nuclear-data uncertainties exist objectively, as the insufficient measurement precision and the modeling uncertainties. The nuclear-data uncertainties have been proved to be one of the most significant sources of uncertainties for the reactor-physics calculations and focused on the increasing attentions recently. The nuclear-data uncertainties are included in the evaluated nuclear-data libraries, such as ENDF/B-VII.1. According to UAM, the uncertainties of the few-group constants should be quantified for the lattice calculations and the uncertainties of the important predictions are focused on for the core simulations.

In order to propagate the nuclear-data uncertainties to the reactor-physics responses, two kinds of methodologies have been proposed and applied widely: the deterministic method and the statistical sampling method. For the deterministic method, the uncertainty analysis is performed using the sandwich formula based on the sensitivity analysis, for which the perturbation theory (PT) and the direct numerical perturbation (DNP) method were widely applied. Comparing the PT and DNP methods, the PT method need to establish different perturbation models for different responses; while for the DNP method, no extra effort is needed for different responses, but larger calculation cost is required than the PT method. For the statistical sampling method (SSM), uncertainty analysis is based on the response samples, which are obtained by the reactor-physics calculations with the corresponding cross-section samples sampled from the nuclear-data uncertainty ranges. With comparisons of the deterministic method and the statistical sampling method for the uncertainty analysis, the PT-based deterministic method has the advantage of high calculation efficiency and the disadvantages of the first-order approximation and of establishing different perturbation models for different responses; the statistical sampling method has the disadvantage of large calculation cost and the obvious advantages of non-linearity and of no limitation or extra efforts for different responses. However, with the increasing development of the computer machine, the computation requirement of the statistical sampling method can be satisfied.

In the context, the SSM has been applied in our-home developed code NECP-UNICORN [2, 3] to perform the uncertainty analysis for the reactor-physics calculations. Based on the "two-step" scheme, the uncertainty-analysis capability for the reactor-physics calculations has been completed in NECP-UNICORN. For the lattice calculations, the nuclear-data uncertainties are firstly propagated to the important responses, including the eigenvalue, few-group constants, kinetic parameters and atomic densities; and then for the core simulations, the few-group constants' uncertainties are propagated to the important responses of the core simulations, including the multiplication factor, power distributions, Boron curve and AO curve. The home-developed code package Bamboo has been coupled in NECP-UNICORN to perform uncertainty analysis to the reactor-physics calculations: Bamboo-Lattice for the lattice calculations and Bamboo-Core for the core calculations. The verifications of NECP-UNICORN have been presented in our previous works [2, 3], and the newly application and researches of NECP-UNICORN for the uncertainty analysis to the BEAVRS [4] benchmark problem has been introduced in detailed in this paper.

1. Overview of the NECP-UNICORN code

Based on the "two-step" scheme for the reactor-physics calculations, the uncertainty-analysis capability has been implemented in our NECP-UNICORN code. Detailed introductions of the theories and methods have been presented and can be found in our previous works. Therefore, the brief introductions of the capabilities of NECP-UNICORN are focused on in this paper. The brief flowchart of NECP-UNICORN applying SSM to perform the uncertainty analysis for the reactor-physics calculations based on the Bamboo code package is shown in Fig. 1.

At the beginning of uncertainty analysis for the lattice calculations, a standard multigroup cross-section format need to be defined by the combined applications of the cross-section information contained in the basic cross-section library and the multigroup microscopic cross-section library with specific format. This standard multigroup cross-section format is designed based on the fact that different lattice codes would utilize different formatted multigroup microscopic cross-section libraries, and with the cross-section information conversion, different lattice codes can be implemented into NECP-UNICORN conveniently when needed. In the standard multigroup cross-section format, the integral, basic and resonance cross sections are defined. The integral cross sections include σ_t, σ_s, σ_a and σ_{tr}; the basic cross sections include $\sigma_{(n,elas)}$, $\sigma_{(n,inel)}$, $\sigma_{(n,2n)}$, $\sigma_{(n,3n)}$, ν, σ_f, σ_γ, $\sigma_{(n,p)}$, $\sigma_{(n,D)}$, $\sigma_{(n,T)}$, $\sigma_{(n,\alpha)}$, $\sigma_{(n,He)}$, $\sigma_{(n,2\alpha)}$ and so on; the resonance

cross sections include σ_t^r, σ_s^r, σ_a^r, σ_f^r, σ_{vf}^r and σ_γ^r. The integral and basic cross sections are defined as the function of the energy groups and temperatures; while the resonance cross sections are defined as function of the energy groups, temperatures and dilution cross sections. Up to now, the cross-section information included in WIMSD-4 [7] formatted library for DRAGON 5.0 [5] and NECL formatted library for Bamboo-Lattice [6] (applying the same kernel theories and methods with NECP-CACTI) can be converted to the cross-section information defined in the standard multigroup cross-section format, and vice versa.

Based on the standard multigroup cross-section format, the verified multigroup cross-section perturbation mode [2] is applied to perturb the multigroup cross sections to the required values according to the relative perturbation factors, which are generated based on the statistical sampling method for the uncertainty analysis. After the cross-section perturbations, the multigroup cross-section consistency rules are applied to keep the integral and basic cross sections balance. This step is essential and important, as correct predictions of the lattice calculations can be obtained only by the balanced and consistent multigroup cross sections. The perturbed cross-section information contained in the standard multigroup cross-section format are then reconstructed into the perturbed multigroup microscopic cross-section library with specific format, e.g. WIMSD-4 and NECL. Provided with the perturbed multigroup microscopic cross-section library, corresponding lattice code is executed to carry out the lattice calculations.

After the lattice calculations based on all of the perturbed multigroup microscopic cross-section libraries, corresponding lattice responses can be obtained. In NECP-UNICORN, a standard responses format is also designed, which can cover the important responses of the lattice calculation, including the eigenvalues, few-group constants, kinetic parameters and atomic densities with the depletions. The responses obtained by the executions of DRAGON5.0 and Bamboo-Lattice can be converted to the standard response format, based on which the uncertainty analysis can be performed. With the statistical sampling method for the lattice calculations, not only the covariance matrices of the few-group constants, but also the samples of the few-group constants can be obtained, based on which the uncertainty analysis for the core simulations can be performed. In this paper, the samples of the few-group constants generated by the uncertainty analysis of the lattice calculations are applied to the uncertainty analysis for the core simulations. The uncertainty information of the important responses for the core simulations can be calculated with the samples of core-simulation responses, obtained by corresponding samples of the few-group constants generated by the uncertainty analysis for the lattice calculations.

The nuclear-data uncertainties can be characterized by the multigroup covariance matrices, which are generated by the NJOY code [11] based on ENDF/B-VII.1 in this paper. Using the relative covariance matrices, the samples of the relative perturbation factors of the multigroup cross sections can be generated as shown in Eq. (1).

$$\mathbf{X}_S = \mathbf{\Sigma}_r^{1/2}\mathbf{Y}_S + \mathbf{1.0} \tag{1}$$

where $\mathbf{\Sigma}_r$ is the relative covariance matrix of the multigroup cross sections; $\mathbf{X}_S$ are the samples of the relative perturbation factors of the multigroup cross sections; $\mathbf{Y}_S$ are the samples of the independent parameters, obeyed the standard normal distributions. For the sampling of $\mathbf{Y}_S$, the technique of Latin Hypercube Sampling (LHS) has been applied in NECP-UNICORN.

The relative covariance matrix $\mathbf{\Sigma}_r$ should be a positive definite matrix, as the square root of $\mathbf{\Sigma}_r$ is required shown in Eq. (1). However, $\mathbf{\Sigma}_r$ is not positive definite sometime. In this case, the eigenvalue decomposition is applied to ensure the $\mathbf{\Sigma}_r$ be positive definite as shown in following.

$$\mathbf{\Sigma}_r = \mathbf{V}\cdot\mathbf{E}\cdot\mathbf{V}^T \tag{2}$$

$$\mathbf{\Sigma}_r^{1/2} = \mathbf{V}\cdot\mathbf{E}^{1/2}\cdot\mathbf{V}^T \tag{3}$$

where $\mathbf{E}$ is the matrix containing the eigenvalue in the diagonal elements. The negative values in $\mathbf{E}$ are replaced by zero to guarantee $\mathbf{\Sigma}_r$ being positive or semi-positive definite matrix.

As the sampling process of the multigroup cross sections is actually the process of adding the perturbations, hence the multigroup cross-section perturbation model has been established and applied in NECP-UNICORN. In this multigroup cross-section perturbation model, the actual perturbations of the multigroup cross sections are propagated form the point-wise cross sections, with considering the perturbations of weighting flux due to the perturbation of the cross sections. The multigroup cross sections are generated from the point-wise cross sections, using the weighting flux shown in Eq. (4).

$$\sigma_{x,g}(T,\sigma_0) = \frac{\int_{\Delta E_g}\sigma_x(E,T)\phi(E,\sigma_0)dE}{\int_{\Delta E_g}\phi(E,\sigma_0)dE} \tag{4}$$

where T, E and σ_0 represent the temperature, energy and background cross section respectively. And $\sigma_x(E,T)$ stands for the energy- and temperature-dependent point-wise cross sections. For the non-resonance cross sections, the weighting flux is the function of energy (formulated as $\phi(E)$), and for the cross sections with resonances, the weighting flux is relative to both energy and background cross sections. And for convenience, the weighting flux is presented as $\phi(E,\sigma_0)$ in following. Since the multigroup cross sections are generated from the point-wise cross sections, the multigroup cross-section perturbations should be consistency with the perturbations propagated from the point-wise cross sections. In this paper, it is assumed that the perturbation for the *gth* group of type *x* is performed by the uniform relative perturbation to the point-wise cross section within the energy range of the *gth* group, shown as in Eq. (5).

$$\sigma_x^{'}(E,T)=(1+\delta_{x,g})\sigma_x(E,T) \quad E_{g-1}\le E\le E_g \tag{5}$$

where $E_{g\text{-}1}$ and E_g present the lower and upper energy boundaries of the *gth* group; $\sigma_x^{'}(E,T)$ stands for the perturbed point-wise cross section of type *x*.

For the cross-section types without resonance, the weighting flux is selected or input by users and independent of the point-wise cross sections. Therefore, the perturbation propagations from the point-wise cross sections to the multigroup ones are linear and can be presented as shown in Eq. (6).

$$\sigma_{x,g}^{'}(T)=\frac{\int_{\Delta E_g}\sigma_x^{'}(E,T)\phi(E)dE}{\int_{\Delta E_g}\phi(E)dE}=(1+\delta_{x,g})\sigma_{x,g}(T) \tag{6}$$

However, for the cross-section types with resonances, the perturbation propagations are non-linear. Because the weighting flux within resonance-energy regions would be perturbed at the same time due to perturbations to the point-wise cross sections. With the NR approximation to the weighting flux, the perturbed resonant cross sections can be characterized as Eq. (7).

$$\begin{aligned}\sigma_{x,g}^{'}(T,\sigma_0)&=\frac{\int_{\Delta E_g}\sigma_x^{'}(E,T)\phi(E,\sigma_0)dE}{\int_{\Delta E_g}\phi(E,\sigma_0)dE}\\&=(1+\delta_{x,g})\frac{\int_{\Delta E_\mu}\sigma_x(\mu,T)\dfrac{\sigma_p^r+\sigma_0}{\sigma_t(\mu,T)+\delta_{x,g}\sigma_x(\mu,T)+\sigma_0}d\mu}{\int_{\Delta E_\mu}\dfrac{\sigma_p^r+\sigma_0}{\sigma_t(\mu,T)+\delta_{x,g}\sigma_x(\mu,T)+\sigma_0}d\mu}\\&=(1+\delta_{x,g})\sigma_{x,g}(T,\sigma_0^{'})\end{aligned} \tag{7}$$

where $\sigma_0^{'}$ stands for the perturbed background cross sections due to perturbations of point-wise cross sections which can be expressed as shown in Eq. (8).

$$\sigma_0^{'}=\frac{\sigma_0}{1+\delta_{t,g}} \tag{8}$$

After the perturbations of the multigroup cross sections, the consistency rules have been implemented to keep the cross sections balance and consistent. Then, the perturbed and consistent multigroup cross sections are converted into the multigroup microscopic cross-section library with the specific format. The consistency rules between the basic cross sections and the integral ones applied in NECP-UNICORN are as shown in following.

$$\sigma_{s,g\to h}=\sigma_{(\mathrm{n,elas}),g\to h}+\sigma_{(\mathrm{n,inel}),g\to h}+2\sigma_{(\mathrm{n,2n}),g\to h}+3\sigma_{(\mathrm{n,3n}),g\to h} \tag{9}$$

$$\begin{aligned}\sigma_{a,g}&=\sigma_{(n,f)}+\sigma_{(n,g)}+\sigma_{(n,\alpha)}+\sigma_{(n,2\alpha)}+\sigma_{(n,\mathrm{p})}+\sigma_{(n,\mathrm{D})}\\&+\sigma_{(n,\mathrm{T})}+\sigma_{(n,\mathrm{He3})}-\sigma_{(n,2n),g}-2\sigma_{(n,3n),g}\end{aligned} \tag{10}$$

$$\sigma_{t,g}=\sigma_{a,g}+\sigma_{s,g} \tag{11}$$

More detailed cross-section consistency rules for different kinds of cross-section perturbations are shown in Table 1~3.

Table 1 Perturbations to basic cross sections without resonance

Basic Cross section	Cross-section Perturbations	Consistency rules
$\sigma_{(\mathrm{n,x})}$(*x*=elas,inel)	$\sigma'_{(\mathrm{n,x}),g}=(1+\delta_{x,g})\sigma_{(\mathrm{n,x}),g}$	$\sigma'_{s,g}=\sigma_{s,g}+\delta_{x,g}\sigma_{(\mathrm{n,x}),g}$
		$\sigma'_{tr,\mathrm{g}}=\sigma_{tr,\mathrm{g}}+\delta_{x,g}\sigma_{(\mathrm{n,x}),\mathrm{g}}$
$\sigma_{(\mathrm{n,2n})}$	$\sigma'_{(\mathrm{n,2n}),g}=(1+\delta_{(\mathrm{n,2n}),g})\sigma_{(\mathrm{n,2n})}$	$\sigma'_{s,g}=\sigma_{s,g}+2\delta_{(\mathrm{n,2n}),g}\sigma_{(\mathrm{n,2n}),g}$
	,*g*	
		$\sigma'_{a,g}=\sigma_{a,g}-\delta_{(\mathrm{n,2n}),g}\sigma_{(\mathrm{n,2n}),g}$
		$\sigma'_{tr,\mathrm{g}}=\sigma_{tr,\mathrm{g}}+\delta_{(\mathrm{n,2n}),g}\sigma_{(\mathrm{n,2n}),g}$
$\sigma_{(\mathrm{n,3n})}$	$\sigma'_{(\mathrm{n,3n}),g}=(1+\delta_{(\mathrm{n,3n}),g})\sigma_{(\mathrm{n,3n})}$	$\sigma'_{s,g}=\sigma_{\mathrm{s,g}}+3\delta_{(\mathrm{n,3n}),g}\sigma_{(\mathrm{n,3n}),g}$
	,*g*	
		$\sigma'_{a,g}=\sigma_{a,\mathrm{g}}-2\delta_{(\mathrm{n,3n}),g}\sigma_{(\mathrm{n,3n}),g}$
		$\sigma'_{tr,\mathrm{g}}=\sigma_{tr,\mathrm{g}}+\delta_{(\mathrm{n,3n}),g}\sigma_{(\mathrm{n,3n}),g}$
$\sigma_{(\mathrm{n,x})}$(*x*=p,D,T,He,α,2α)	$\sigma'_{(\mathrm{n,x}),g}=(1+\delta_{x,g})\sigma_{(\mathrm{n,x}),g}$	$\sigma'_{a,\mathrm{g}}=\sigma_{a,\mathrm{g}}+\delta_{x,\mathrm{g}}\sigma_{(\mathrm{n,x}),g}$
		$\sigma'_{tr,\mathrm{g}}=\sigma_{tr,\mathrm{g}}+\delta_{x,\mathrm{g}}\sigma_{(\mathrm{n,x}),g}$

Table 2 Perturbations to basic cross sections with resonance

Cross section	Cross-section Perturbations	Consistency rules
$\sigma_{(\mathrm{n},f)}$	$\sigma'_{(\mathrm{n},f),g}=(1+\delta_{(\mathrm{n},f),g})\sigma_{(\mathrm{n},f),g}$	$\sigma'_{tr,\mathrm{g}}=\sigma_{tr,\mathrm{g}}+\delta_{(\mathrm{n},f),g}\sigma_{(\mathrm{n},f),g}$
		$\sigma'_{a,\mathrm{g}}=\sigma_{a,\mathrm{g}}+\delta_{(\mathrm{n},f),g}\sigma_{(\mathrm{n},f),g}$
		$\sigma_{vf,g}=\nu(1+\delta_{(\mathrm{n},f),g})\sigma_{(\mathrm{n},f),g}$
		$I'_{a,g}(T,\sigma_0)=\sigma'_{a,\mathrm{g}}(T,\sigma'_0)\sigma_0/(\sigma'_{a,\mathrm{g}}(T,\sigma'_0)+\sigma_0)$
		$I'_{vf,g}=\sigma'_{vf,\mathrm{g}}(T,\sigma'_0)\sigma_0/(\sigma'_{a,\mathrm{g}}(T,\sigma'_0)+\sigma_0)$
$\sigma_{(\mathrm{n},\gamma)}$	$\sigma'_{(\mathrm{n},\gamma),g}=(1+\delta_{(\mathrm{n},\gamma),g})\sigma_{(\mathrm{n},\gamma),g}$	$\sigma'_{tr,\mathrm{g}}=\sigma_{tr,\mathrm{g}}+\delta_{(\mathrm{n},\gamma),g}\sigma_{(\mathrm{n},\gamma),g}$
		$\sigma'_{a,g}=\sigma_{a,\mathrm{g}}+\delta_{(\mathrm{n},\gamma),g}\sigma_{(\mathrm{n},\gamma),g}$
		$I'_{a,g}(T,\sigma_0)=\sigma'_{a,g}(T,\sigma'_0)\sigma_0/(\sigma'_{a,g}(T,\sigma'_0)+\sigma_0)$
		$I'_{vf,g}=\sigma_{vf,g}(T,\sigma'_0)\sigma_0/(\sigma'_{a,g}(T,\sigma'_0)+\sigma_0)$

Table 3 Perturbations to total cross section within resonance groups

Cross section	Cross-section Perturbations	Consistency rules
σ_t	$\sigma'_{t,g}=(1+\delta_{t,g})\sigma_{t,g}$	$I'_{a,g}(T,\sigma_0)=\sigma_{a,g}(T,\sigma'_0)\sigma_0/(\sigma_{a,g}(T,\sigma'_0)+\sigma_0)$
		$I'_{vf,g}=\sigma_{vf,g}(T,\sigma'_0)\sigma_0/(\sigma_{a,g}(T,\sigma'_0)+\sigma_0)$

With the perturbed or samples of the multigroup microscopic cross-section libraries, the lattice calculations are carried out to obtain the samples of the responses. For the lattice calculations, the response types include the eigenvalue, few-group constants, kinetic parameters and atomic densities; for the steady-stated core simulations, the response types include the multiplication factor and power distributions. The uncertainty information of the interested responses can be quantified using these responses' samples as shown in Eq. (12).

$$\boldsymbol{\Sigma}_{\boldsymbol{R},i,j}=\frac{1}{nS-1}\sum_{n=1}^{nS}(R_{i,n}-R_{i,0})(R_{j,n}-R_{j,0}) \tag{12}$$

where *nS* is the size of the samples; $\boldsymbol{\Sigma}_{\boldsymbol{R}}$ represents the covariance matrix of responses with the size of $nR\times nR$; $\boldsymbol{\Sigma}_{\boldsymbol{R},i,j}$ is the covariance for the *ith* and *jth* response ($i,j=1,2,\ldots,nR$); $R_{i,n}$ (or $R_{j,n}$) and $R_{i,0}$ (or $R_{j,0}$) stand for the *nth* sample value and expectation value for the *ith* (or *jth*) response R_i (or R_j), which can be characterized as shown in Eq. (13).

$$R_{i,0} = \frac{1}{nS}\sum_{n=1}^{nS} R_{i,n} \tag{13}$$

In the covariance matrix $\boldsymbol{\Sigma_R}$, the square roots of the diagonal elements represent the uncertainties of corresponding responses, and the off-diagonal elements stand for the correction coefficient of corresponding two responses.

As the fact that for the statistical sampling method, the statistical errors are inevitable to the uncertainty results because the number of samples is a specific but not infinite number. Therefore, the bootstrap method [12] has been applied to evaluate the confidence intervals for the uncertainty results. For the purpose of evaluating the confidence interval for uncertainties results of uncertainty analysis, resampling technology is used and series of re-samples are generated to perform the uncertainty analysis. The uncertainty of *ith* re-samples for the *kth* response can be presented as $\sigma(R_k)_i$ (i=1,2,…,N) where N is the total number of re-samples, and the bootstrap confidence interval can be quantified by formula as Eq.

$$\Delta\sigma(R_k) = \sqrt{\frac{1}{N-1}\sum_{i=1}^{N}(\sigma(R_k)_i - \sigma(R_k)_0)^2} \tag{14}$$

where $\Delta\sigma(R_k)$ presents the deviation of the uncertainty results by application of the N re-samples; $\sigma(R_k)_i$ is the uncertainty result of the ith re-samples, and $\sigma(R_k)_0$ presents the expectation value of the N uncertainty results which can be formulated shown as in Eq.

$$\sigma(R_k)_0 = \frac{1}{N}\sum_{i=1}^{N}\sigma(R_k)_i \tag{15}$$

In the process of uncertainty analysis for the lattice calculations, the samples of the few-group constants can be obtained. Therefore, these samples are directly provided to the uncertainty analysis for the core simulations. This method has the advantage of no requirement to re-sample for the few-group constants. Our home-developed core code Bamboo-Core [8] has been added into NECP-UNICORN to carry out the steady-stated core simulations.

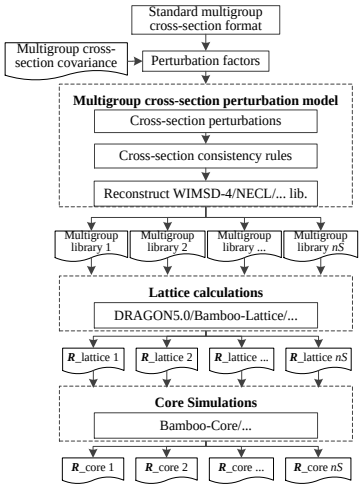

Fig. 1. The brief flowchart of NECP-UNICORN

2. Numerical Results and Analysis

In this paper, NECP-UNICORN has been applied to the uncertainty analysis for the BEAVRS benchmark problem. The uncertainty analysis has been performed to the HZP condition of BEAVRS with the simulations of ARI and ARO. Our home-developed Bamboo-Lattice and Bamboo-Core are applied to perform the steady-stated modeling and simulation of BEAVRS based on the "two-step" scheme in NECP-UNICORN. For the lattice calculations, the relative uncertainties of the eigenvalue and two-group constants (with cut-off energy for the fast and thermal group set to be 0.625eV) are quantified; for the steady-stated core simulations, the relative uncertainties of the multiplication factor and power distributions are determined. Before the uncertainty analysis to the BEAVRS benchmark, verification of modeling and simulations for the BEAVRS benchmark based on Bamboo-Lattice and Bamboo-Core has been performed.

A. Modeling and Simulation of BEAVRS

Verifications of the modeling and simulation with coupled application of Bamboo-Lattice and Bamboo-Core are performed based on the ARO situation. For the ARO situation of BEAVRS at HZP, there are 9 different kinds of fuel assemblies. Using the essential parameters for modeling and simulation published by MIT, including the geometry, temperature, isotope compositions and the configurations, the lattice calculations for these fuel assemblies are modeled and simulated by both Bamboo-Lattice and CASMO-4E [9]. The eigenvalues of these fuel assemblies are compared in Table 4.

Table 4. Eigenvalues of the fuel assemblies of BEAVRS at HZP with ARO

	CASMO-4E	Bamboo-Lattice	Difference/pcm
16000	0.98952	0.98944	-8
24000	1.13130	1.13127	-3
24012	1.00857	1.00837	-20
24016	0.97033	0.97039	6
31000	1.21279	1.21269	-10
31006	1.15630	1.15614	-16
31015	1.07251	1.07253	2
31016	1.05786	1.05793	7
31020	1.02229	1.02256	27

It can be observed that the differences in eigenvalues of the fuel assemblies between Bamboo-Lattice and CASMO-4E are all within 30pcm, which is small and acceptable. These comparisons assure that the modeling and simulations for the fuel assemblies of BEAVRS Bamboo-Lattice are correct.

For the verification of the steady-stated core simulation, the radial power distributions obtained by Bamboo-Lattice and Bamboo-Core are compared with those by CASMO-4E and CASMO5. The radial power distributions by CASMO-

4E are obtained using the "one-step" neutron-transport simulation of the whole core, and the results by CASMO5 are done and published by the Idaho National Laboratory (INL) [10]. For the steady-stated core simulations, the multiplication factor obtained by Bamboo-Core is 0.99977 (-23pcm), compared with this by the "one-step" neutron-transport result by CASMO-4E be 1.00031 (+31pcm). The assembly power distributions obtained by Bamboo-Core, CASMO-4E and CASMO5 are compared and shown in Fig. 2. The RMS percent difference of the radial power distributions is 0.91% between Bamboo-Core and CASMO-4E and 0.86% between Bamboo-Core and CASMO5. For the "two-step" scheme for the core simulations, these differences are acceptable. Therefore, applying our home-developed Bamboo-Lattice and Bamboo-Core, the correct modeling and simulations of BEAVRS at HZP can be implemented. Moreover, the same modeling and simulations have been applied for the ARI situation, adding the fuel assemblies with the insertion of the control rods and the critical boron concentration set to be 686ppm according to the operation data of BEAVRS.

0.709	0.801	0.804	0.971	0.872	0.966	0.939	1.004
0.699	0.789	0.796	0.960	0.868	0.965	0.948	1.019
-1.4	-1.5	-1.0	-1.1	-0.5	-0.1	1.0	1.5
0.801	0.767	0.938	0.868	1.007	0.900	1.133	1.065
0.789	0.758	0.924	0.862	0.998	0.902	1.135	1.065
-1.5	-1.2	-1.5	-0.7	-0.9	0.2	0.2	0.0
0.804	0.938	0.864	1.022	0.913	1.010	0.941	0.939
0.796	0.924	0.858	1.012	0.912	1.010	0.948	0.955
-1.0	-1.5	-0.7	-1.0	-0.1	0.0	0.7	1.7
0.971	0.868	1.022	0.951	1.095	1.024	1.187	0.779
0.960	0.862	1.012	0.951	1.096	1.031	1.187	0.776
-1.1	-0.7	-1.0	0.0	0.1	0.7	0.0	-0.4
0.872	1.007	0.913	1.095	1.444	1.193	1.269	
0.868	0.998	0.912	1.096	1.442	1.207	1.262	
-0.5	-0.9	-0.1	0.1	-0.1	1.2	-0.6	
0.966	0.900	1.010	1.024	1.193	1.250	0.936	
0.965	0.902	1.010	1.031	1.207	1.280	0.936	
-0.1	0.2	0.0	0.7	1.2	2.4	0.0	
0.939	1.133	0.941	1.187	1.269	0.936		
0.948	1.135	0.948	1.187	1.262	0.936		
1.0	0.2	0.7	0.0	-0.6	0.0		
1.004	1.065	0.939	0.779			CASMO-4E	
1.019	1.065	0.955	0.776			Bamboo-Lattice+Core	
1.5	0.0	1.7	-0.4			Difference/%	

(a). Comparison between Bamboo and CASMO-4E

0.698	0.791	0.795	0.962	0.866	0.965	0.939	0.992
0.699	0.789	0.796	0.96	0.868	0.965	0.948	1.019
0.1	-0.3	0.1	-0.2	0.2	0.0	1.0	2.7
0.791	0.757	0.927	0.86	1.002	0.899	1.134	1.051
0.789	0.758	0.924	0.862	0.998	0.902	1.135	1.065
-0.3	0.1	-0.3	0.2	-0.4	0.3	0.1	1.3
0.795	0.927	0.857	1.017	0.911	1.014	0.945	0.933
0.796	0.924	0.858	1.012	0.912	1.01	0.948	0.955
0.1	-0.3	0.1	-0.5	0.1	-0.4	0.3	2.4
0.962	0.86	1.017	0.951	1.103	1.033	1.196	0.776
0.96	0.862	1.012	0.951	1.096	1.031	1.187	0.776
-0.2	0.2	-0.5	0.0	-0.6	-0.2	-0.8	0.0
0.866	1.002	0.911	1.103	1.452	1.216	1.276	
0.868	0.998	0.912	1.096	1.442	1.207	1.262	
0.2	-0.4	0.1	-0.6	-0.7	-0.7	-1.1	
0.965	0.899	1.014	1.033	1.216	1.27	0.944	
0.965	0.902	1.01	1.031	1.207	1.28	0.936	
0.0	0.3	-0.4	-0.2	-0.7	0.8	-0.8	
0.939	1.134	0.945	1.196	1.276	0.944		
0.948	1.135	0.948	1.187	1.262	0.936		
1.0	0.1	0.3	-0.8	-1.1	-0.8		
0.992	1.051	0.933	0.776			CASMO 5 by INL	
1.019	1.065	0.955	0.776			Bamboo-Lattice+Core	
2.7	1.3	2.4	0.0			Difference / %	

(b). Comparison between Bamboo and CASMO 5

Fig. 2. The comparison of the assembly power distributions

Based on the correct modeling and simulations for the BEAVRS benchmark using Bamboo-Lattice and Bamboo-Core, uncertainty analysis has been performed to the HZP conditions with the situations of ARO and ARI.

B. Uncertainty Results for the Lattice Calculations

For the lattice calculations, the relative uncertainties of the eigenvalues and two-group constants have been quantified for the fuel assemblies. The size of samples N_S is 2000 (10 re-sample with sample size to be 200) in the uncertainty analysis for the lattice calculation and hence for the steady-stated core simulation. The nuclides and corresponding cross-section types analyzed in the uncertainty analysis for the lattice calculations are listed and shown in Table 5. The uncertainty-analysis results and corresponding standard errors of the lattice calculation for the fuel assemblies are shown in Table 6 for the ARO situation and Table 7 for the ARI situation. In Table 6 and Table 7, 31000, 31006, 31015, 31016, 31020, 24000, 24012, 24016, 16000, 16000R and 24000R represent the fuel assemblies 3.1% with 0 BA, 3.1% with 6 BA, 3.1% with 15 BA, 3.1% with 16 BA, 3.1% with 20 BA, 2.4% with 0 BA, 2.4% with 12 BA, 2.4% with 16 BA, 1.6% with 0 BA, 1.6% with control rods and 2.4% with control rods, where the percentage stands for the enrichment of ^{235}U and BA represents the burnable absorber.

Table 5. The nuclides and cross-section types analyzed

Cross section	Nuclides analyzed
$\sigma_{(n,elas)}$	^{234}U,^{235}U,^{238}U,^{1}H,^{16}O,^{90}Zr,^{91}Zr,^{92}Zr,^{10}B,^{11}B
$\sigma_{(n,inel)}$	^{234}U,^{235}U,^{238}U,^{90}Zr,^{91}Zr,^{92}Zr,^{10}B,^{11}B
$\sigma_{(n,2n)}$	^{234}U,^{235}U,^{238}U,^{90}Zr,^{91}Zr,^{92}Zr
σ_f	^{234}U,^{235}U,^{238}U
σ_γ	^{234}U,^{235}U,^{238}U,^{1}H,^{16}O,^{90}Zr,^{91}Zr,^{92}Zr,^{10}B,^{11}B
ν	^{235}U,^{238}U
σ_α	^{16}O,^{10}B,^{11}B

It can be observed that the relative uncertainties for the eigenvalues of the fuel assemblies vary from 5.0‰ to 5.8‰; and the largest relative uncertainties of the two-group constants can up to be 1.70% for D_1, the fast-group diffusion coefficient. Moreover, the relative uncertainties of the fast-group constants are larger than those of the thermal group. The response uncertainties at ARO situation almost have the same magnitude with those at ARI situation.

Table 6. Uncertainty-analysis results and corresponding standard errors with ARO situation

	16000/%	24000/%	24012/%	24016/%	31000/%	31006/%	31015/%	31016/%	31020/%
k_∞	0.57±0.02	0.52±0.02	0.52±0.02	0.52±0.02	0.50±0.02	0.50±0.02	0.50±0.02	0.50±0.02	0.50±0.02
D_1	1.65±0.11	1.62±0.11	1.64±0.11	1.65±0.11	1.60±0.11	1.61±0.11	1.62±0.11	1.63±0.11	1.63±0.11
D_2	0.37±0.02	0.37±0.02	0.37±0.02	0.37±0.02	0.37±0.02	0.37±0.02	0.37±0.02	0.37±0.02	0.37±0.02
$\Sigma_{a,1}$	1.02±0.06	0.96±0.05	0.96±0.05	0.96±0.05	0.92±0.05	0.92±0.05	0.92±0.05	0.93±0.05	0.93±0.05
$\Sigma_{a,2}$	0.44±0.02	0.39±0.01	0.34±0.01	0.33±0.01	0.36±0.01	0.34±0.01	0.32±0.01	0.31±0.01	0.30±0.01
$\nu\Sigma_{f,1}$	1.03±0.05	0.76±0.04	0.76±0.04	0.75±0.04	0.64±0.03	0.63±0.03	0.63±0.03	0.63±0.03	0.62±0.03
$\nu\Sigma_{f,2}$	0.39±0.01	0.38±0.01	0.38±0.01	0.38±0.01	0.38±0.01	0.38±0.01	0.38±0.01	0.38±0.01	0.38±0.01
$\Sigma_{s,1,1}$	1.01±0.06	1.01±0.06	1.01±0.06	1.02±0.06	1.00±0.06	1.00±0.06	1.01±0.06	1.01±0.06	1.01±0.06
$\Sigma_{s,1,2}$	1.18±0.06	1.11±0.06	1.18±0.06	1.21±0.06	1.08±0.06	1.11±0.06	1.16±0.06	1.16±0.06	1.18±0.06
$\Sigma_{s,2,1}$	0.57±0.03	0.55±0.03	0.53±0.03	0.53±0.03	0.54±0.03	0.54±0.03	0.52±0.03	0.52±0.03	0.52±0.03
$\Sigma_{s,2,2}$	0.35±0.02	0.35±0.02	0.36±0.02	0.36±0.02	0.35±0.02	0.36±0.02	0.36±0.02	0.36±0.02	0.36±0.02

Table 7. Uncertainty-analysis results and corresponding standard errors with ARI situation

	16000/%	24000/%	24012/%	24016/%	31000/%	31006/%	31015/%	31016/%	31020/%	**16000R/%**	**24000R/%**
k_∞	0.58±0.03	0.53±0.02	0.52±0.02	0.52±0.02	0.51±0.02	0.50±0.02	0.50±0.02	0.50±0.02	0.50±0.02	0.57±0.02	0.53±0.02
D_1	1.64±0.11	1.61±0.11	1.63±0.11	1.64±0.11	1.59±0.11	1.60±0.11	1.62±0.11	1.62±0.11	1.63±0.11	1.70±0.11	1.66±0.11
D_2	0.37±0.02	0.37±0.02	0.37±0.02	0.37±0.02	0.37±0.02	0.37±0.02	0.37±0.02	0.37±0.02	0.37±0.02	0.36±0.02	0.36±0.02
$\Sigma_{a,1}$	1.02±0.06	0.96±0.05	0.96±0.05	0.96±0.05	0.92±0.05	0.92±0.05	0.92±0.05	0.92±0.05	0.93±0.05	1.05±0.06	0.98±0.06
$\Sigma_{a,2}$	0.46±0.02	0.41±0.01	0.36±0.01	0.34±0.01	0.37±0.01	0.37±0.01	0.33±0.01	0.32±0.01	0.31±0.01	0.31±0.01	0.29±0.01
$\nu\Sigma_{f,1}$	1.03±0.06	0.76±0.04	0.76±0.04	0.76±0.04	0.64±0.03	0.64±0.03	0.63±0.03	0.63±0.03	0.63±0.03	1.08±0.06	0.77±0.04
$\nu\Sigma_{f,2}$	0.39±0.01	0.38±0.01	0.38±0.01	0.38±0.01	0.38±0.01	0.38±0.01	0.38±0.01	0.38±0.01	0.38±0.01	0.39±0.01	0.38±0.01
$\Sigma_{s,1,1}$	1.01±0.07	1.00±0.06	1.00±0.06	1.01±0.06	1.00±0.06	1.00±0.06	1.01±0.06	1.01±0.06	1.01±0.06	1.02±0.06	1.00±0.06
$\Sigma_{s,1,2}$	1.15±0.06	1.09±0.06	1.16±0.06	1.19±0.06	1.06±0.05	1.09±0.06	1.14±0.06	1.15±0.06	1.17±0.06	1.49±0.08	1.38±0.07
$\Sigma_{s,2,1}$	0.59±0.03	0.56±0.03	0.54±0.03	0.53±0.03	0.55±0.03	0.54±0.03	0.53±0.03	0.53±0.03	0.52±0.03	0.51±0.03	0.50±0.03
$\Sigma_{s,2,2}$	0.35±0.02	0.35±0.02	0.36±0.02	0.36±0.02	0.35±0.02	0.36±0.02	0.36±0.02	0.36±0.02	0.36±0.02	0.36±0.02	0.36±0.02

Uncertainty Results for the Core Simulations

Provided with the samples of the two-group constants for the fuel assemblies at both the ARO and ARI situations, uncertainty analysis have been performed to the steady-stated core simulations. The relative uncertainties of the multiplication factor of BEAVRS at HZP are shown in Table 8.

Table 8. Relative uncertainties of the multiplication factor

Situation	*keff*	$\Delta k_{eff}/k_{eff}$/%
ARO	0.99977	0.51
ARI	0.99921	0.50

It can be observed that the relative uncertainties of the multiplication factors are 5.1‰ for the ARO situation and 5.0‰ for the ARI situation, with the same magnitude of the relative uncertainties of the eigenvalues for the fuel assemblies.

The relative uncertainties of the power distributions in both ARO and ARI situations are compared and shown in Fig. 3.

0.699	0.789	0.796	0.960	0.868	0.965	0.948	1.019
4.27	3.98	3.47	2.68	1.91	0.70	0.66	1.69
0.789	0.758	0.924	0.862	0.998	0.902	1.135	1.065
3.98	3.82	3.21	2.60	1.66	0.62	0.89	1.79
0.796	0.924	0.858	1.012	0.912	1.010	0.948	0.955
3.47	3.21	2.80	2.02	1.27	0.16	0.99	1.87
0.960	0.862	1.012	0.951	1.096	1.031	1.187	0.776
2.68	2.60	2.02	1.30	0.28	0.59	1.63	1.93
0.868	0.998	0.912	1.096	1.442	1.207	1.262	
1.91	1.66	1.27	0.28	0.83	1.55	2.23	
0.965	0.902	1.010	1.031	1.207	1.280	0.936	
0.70	0.62	0.16	0.59	1.55	2.28	2.52	
0.948	1.135	0.948	1.187	1.262	0.936		
0.66	0.89	0.99	1.63	2.23	2.52		
1.019	1.065	0.955	0.776			Assembly Power	
1.69	1.79	1.87	1.93			Rel. Unc./%	

(a). For ARO situation

0.176	0.381	0.297	0.980	1.090	0.981	0.416	0.851
6.03	5.23	4.39	2.79	2.31	1.95	1.33	0.64
0.381	0.436	0.623	0.916	1.240	0.969	0.877	0.914
5.23	4.78	3.81	2.71	2.03	1.68	0.65	0.84
0.297	0.623	0.376	1.050	1.120	1.070	0.476	0.910
4.39	3.81	3.58	2.22	1.59	0.84	0.42	1.39
0.980	0.916	1.050	1.030	1.140	1.200	1.340	0.882
2.79	2.71	2.22	1.71	0.78	0.65	1.88	2.04
1.090	1.240	1.120	1.140	0.787	1.430	1.790	
2.31	2.03	1.59	0.78	0.43	2.12	2.99	
0.981	0.969	1.070	1.200	1.430	1.780	1.450	
1.95	1.68	0.84	0.65	2.12	3.16	3.44	
0.416	0.877	0.476	1.340	1.790	1.450		
1.33	0.65	0.42	1.88	2.99	3.44		
0.851	0.914	0.910	0.882			Assembly Power	
0.64	0.84	1.39	2.04			Rel. Unc./%	

(b). For ARI situation

Fig. 3. The relative uncertainties of the power distributions

It can be observed that the relative uncertainties of the power distributions at ARI are larger than those at ARO. For the situation of ARO, the maximum relative uncertainty is 4.27% occurred in the middle assembly, and the RMS value of the relative uncertainties is 2.08%; for the situation of ARI, the maximum relative uncertainty is 6.03% occurred in the middle assembly, and the RMS value of the relative uncertainties is 2.37%.

From the view of the reactor-physics calculations, the uncertainties of the multiplication factor and power distributions introduced by the nuclear-data uncertainties are notable. Moreover, the uncertainties are expected higher for the depleted core at HFP than those for the fresh-fueled core at HZP. Therefore, these nuclear-data uncertainties should be taken into account for the safety analysis and economic competitiveness of the reactor system.

III. CONCLUSIONS

In this paper, the uncertainty-analysis capability for the reactor-physics calculations based on the "two-step" scheme has been implemented in our home-developed NECP-UNICORN code. The nuclear-data uncertainties are firstly propagated to the important responses of the lattice calculations, including the eigenvalue, few-group constants, kinetic parameters and atomic densities with depletions; and then to the significant responses of the core simulations, including the multiplication factor, power distributions Boron curve and AO curve. With NECP-UNICORN, the uncertainty analysis has been performed to the BEAVRS benchmark problem at the HZP condition with the ARO and ARI situations. The relative uncertainties of the eigenvalue and few-group constants for the lattice calculations and multiplication factor and power distributions for the steady-state core simulations have been quantified. Notable uncertainties can be observed for the important responses of the reactor-physics calculations for the fresh-fueled core, these uncertainties will be higher for the depleted core. Therefore, the uncertainty analysis will be focused on the cycle calculations and transient calculations in the further researches.

ACKNOWLEDGEMENTS

This work is supported by the National Natural Science Foundation of China (Grant No. 11522544, 11605128).

REFERENCES

1. Ivanov, K., Avramova, M., Kamerow, S., Kodeli, I., Sartori, E., Ivanov, E., Cabellos, O., 2013. Benchmarks for Uncertainty Analysis in Modelling (UAM) for the Design, Operation and Safety Analysis of LWRs. OECD Nuclear Energy Agency, NEA/NSC/ DOC(2013)7.
2. Wan, C., Cao, L., Wu, H., et al., 2015. Code development for eigenvalue total sensitivity analysis and total uncertainty analysis. Annals of Nuclear Energy 85, 788-797.
3. Zu, T., Wan, C., Cao, L., et al., 2016. Total Uncertainty Analysis for PWR Assembly Based on the Statistical Sampling method. Nuc. Sci. & Eng, 183: 371-386.
4. Horelik, N., Herman, B., 2013. Benchmark for Evaluation And Validation of Reactor Simulations rev. 1.1.1. MIT Computational Reactor Group (2013).
5. Marleau G., Hébert A., Roy R., 2014. A User Guide for DRAGON Version 5. Technical Report, IGE-335.
6. Li, Y., Tian, C., Zheng, Y., et al., 2015. NECP-CACTI: Pressurized Water Reactor Lattice Code Development, Transactions of the American Nuclear Society, vol. 112, San Antonio.
7. Leszczynski F., Aldama D. L., Trkov A., 2007. WIMS-D Library Update: Final Report of a Coordinated Research Project. International Atomic Energy Agency.
8. Li, Y., Wang, Y., Liang, B., Shen, W., 2015b. Partitioned-Matrix acceleration to the Fission-Source iteration of the Variational Nodal Method. Progress in Nuclear Energy, 85: 640-647.
9. Rhodes, J., Smith, K., Edenius, M., 2004. CASMO-4E: Extended Capability CASMO-4, User's Manual. Studsvik Scandpower, Report SSP-09/443 University Release.
10. Ellis, M., Ortensi, J., Wang, Y., et al., 2014. Initial RattleSnake Calculations of the Hot Zero Power BEAVRS. Massachusetts Institute of Technology, INL/EXT-13-30903.
11. Macfarlane R. E., Muir D. W., Boicourt R. M., et al., 2012. The NJOY Nuclear Data Processing System, Version 2012. Los Alamos National Security, LA-UR-12-27079.
12. Archer G. E. B., Saltelli A., Sobol I. M., 1997. Sensitivity Measures, Anova-like Techniques and the Use of Bootstrap. Journal of Statistical Computation and Simulation, Vol. 58: 99-120.